Nonparametric identification of a small AMB test rig at several rotating speeds

Diego Diaz [a], Fernando Pinto [b], Thiago Ritto [c], David Maldonado [d], Vinicius Côrtes [e]

Av. Horacio Macedo 2030 Centro de Tecnologia Bl. i-130, Acoustics and Vibrations Laboratory (LAVI), Federal University of Rio de Janeiro, Rio de Janeiro, Brasil. [a] dgodoy@ufrj.br, [b] fcpinto@ufrj.br, [c] tritto@mecanica.ufrj.br, [d] davidjuliang@hotmail.com, [e] viniciuscortes@poli.ufrj.br

***Abstract*— In this paper a comparison of experimental frequency response functions (FRFs) obtained in a small-scale Active Magnetic Bearing (AMB) test rig at several rotating speeds is made, in order to assess the gyroscopic and shaft unbalances effects in practical identification procedures. The excitation frequencies used in this work were established below the critical speed (rigid rotor behavior) and a broadband signal is used as excitation input.**

I. INTRODUCTION

Identification of Active Magnetic Bearings (AMBs) is an essential step when a model calibration of a system that uses such technology is required. Turbocompressors are one of the most common applications where AMBs became an interesting solution, offering the ability not only of supporting and controlling but also shaking the shaft for identification purposes [1].

Perhaps one of the first works of rotordynamic systems identification using magnetic bearings was presented by Nordmann et. al. [2]. In that paper, the authors highlighted the advantages of contactless input techniques, and the wide broadband possibilities of signal excitation when controlled magnetic forces are used. Two industrial-scale test rigs supported by AMBs are known in literature because of their high pressure capability (250 Bar). The first was developed by Siemens [3] and years later the second was devised by GE [4]. Both test rigs were used to assess labyrinth seals with Nitrogen as gas test.

On the academic side, various small-scale test rigs were tested. Regarding the identification procedures, Gälher and erzog [5] proposed a parametric identification method for a SISO AMB system and then extended it to MIMO flexible rotor systems [6]. A variant of previous model, particularly for obtaining the rigid modes was proposed by Ahn et. al. [7], yielding numerous experiment results with an indoor AMB test apparatus. Hynynen [8] made a detailed study of AMB identification using broadband waveforms as excitation signals, that is, using a set of harmonic signals superposed with different frequency and phase.

In those previous works, the gyroscopic and unbalancing effects were neglected, or tests were performed at nonrotating condition. In this work the frequency response functions (FRFs) were obtained from a previous small-scale test rig and compared with various shaft rotating speeds using a broadband type signal.

II. IDENTIFICATION PROCEDURE

Due to its good performance in noise presence [9], identification is generally made in the frequency domain, that is, the use of frequency response function (FRF). Basically, this method consists in an excitation applied in a system while its inputs and outputs are measured by means of sensors or transductors. These measurements are treated and stored by a data acquisition system (DAQ) with a proper anti-alias filter, and then processed by an algorithm that computes their Discrete Fourier Transform, implemented a Fast Fourier Transform (FFT) [2], as shown in Figure 1. Finally, the ratio of the outputs and inputs are defined as the FRF.

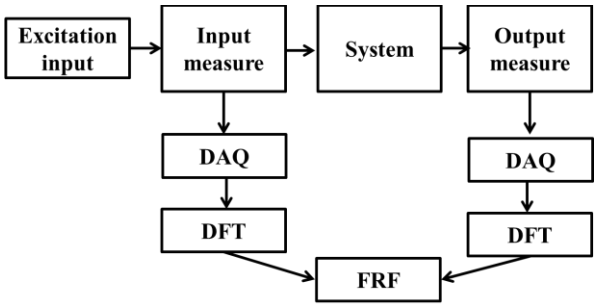

Figure 1. Block diagram for identification using FRF method [17]

In the case of an Active Magnetic Bearing system, the closed loop system is presented in Figure 2. As first step, the setpoints in the AMB multiple input-output system (MIMO) are established, being commonly the magnetic center of each actuator arrangement. The controller scheme determines the equivalent value to each amplifier input, whose principal function is to provide the necessary current in the coils to keep the rotor as close as possible of the setpoints values (i.e. levitating). The power amplifier block usually includes the electrical impedance of the coils and the respective electronic devices model [10]. An excitation is added to the control signal aiming to generate a system perturbation, and the perturbation currents u are calculated from the measured coil currents. In parallel, the relative system positions y are measured and stored in the DAQ device. Since the identification is made in

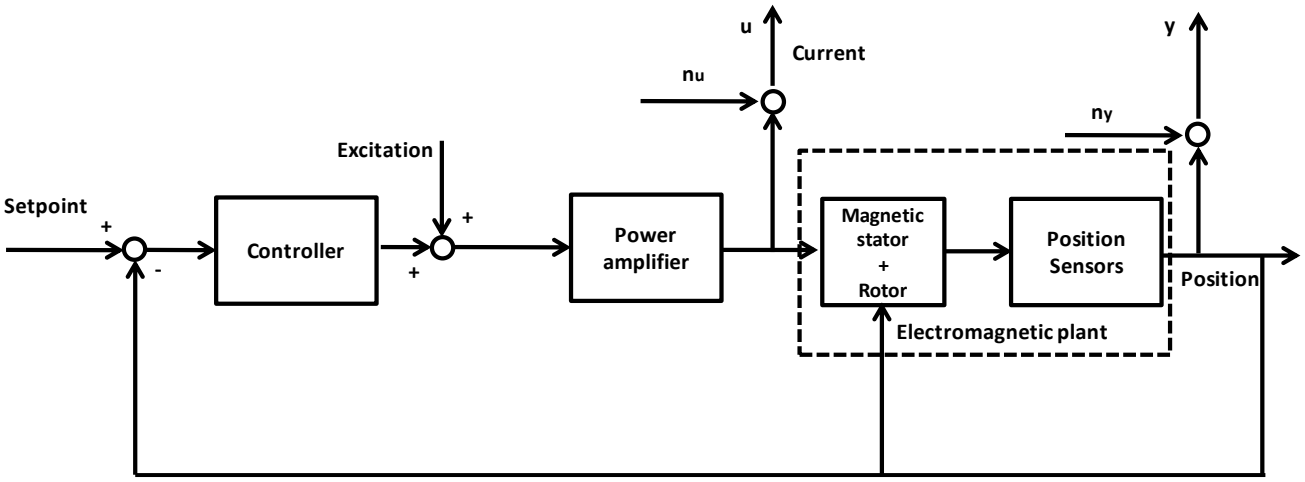

Figure 2. AMB block diagram (modified) [10]

the frequency domain, periodic signals are preferred as excitation input, whose major benefit is the leakage reduction.

A noise is present in the calculated perturbation currents u (plant inputs) and measured outputs y are added as n_u and n_y respectively. For this work, the feedback propagation noise is neglected, and it is assumed that exist an independence between the input and output noise, namely:

$$\mathbb{E}\{N_Y(\omega_k)N_U(\omega_k)\} = 0 \qquad (2)$$

where ω_k is the k-th frequency of the input N_U and output spectrum N_Y. With a typical differential in "*horseshoe*" arrangement, as shown in Figure 3, a linearization with a bias current i_o and nominal air gap g_0 is feasible. Such a configuration facilitates the control implementation since the force is practically exerted in a single radial axis, and the magnetic flux path is maintained in the same magnet quadrant when the poles are symmetric.

The excitation S_e and the control signal S_x are summed and subtracted from the bias signal s_0 in the upper and lower electromagnets respectively. If a linear behavior is present in the amplifiers, or at least in their operation bandwidth, one can expect a linear equivalent current output in each coil, being the bias current i_o, control current i_x and excitation current i_e. The contribution of the control and excitation currents is denoted as the input signal of the system (i.e. $u = i_p = i_x + i_e$).

In the cases where the perturbation current cannot be measured directly (e.g. amplifiers without feedback loop control), an estimation of that value can be obtained by measuring the coil currents, that is:

$$i_1 = i_0 + i_p = i_0 + i_x + i_e \qquad (3)$$

$$i_3 = i_0 - i_p = i_0 - i_x - i_e \qquad (4)$$

Combining Equation 3 and Equation 4 yields:

$$i_p = \frac{i_1 - i_3}{2} \qquad (5)$$

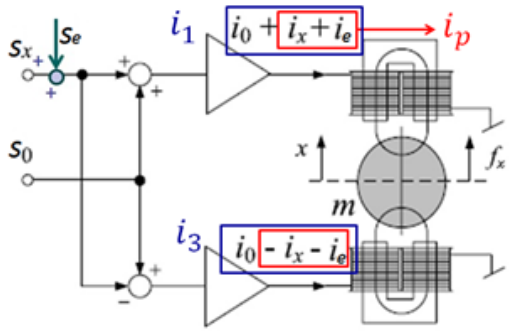

Figure 3. Electromagnret with horseshoe differential configuration (modified) [10]

In the same sense, the bias current is estimated averaging the upper and lower coil currents measurements, expressed as follows:

$$i_0 = \frac{i_1 + i_3}{2} \qquad (6)$$

A. *FRF Averaging*

As the noise is an inherent phenomena present in experimental processes, several repetitions (or blocks) of the experiment ought to be performed, in order to increase the SNR and compensate any inadequate non stationary effect during the test procedure. Pintelon et. al. [11] present a very detailed state of art for averaging ways (also known as estimators) in the frequency domain.

In the spirit of Hynynen's work [8], Diaz et. al. [12] performed tests with an indoor small AMB test rig, in order to obtain the FRFs using several estimators and excitation signals. In that paper, those tests were performed only in the vertical direction with nonrotating condition, aiming to obtain the relation between the two radial actuators where their shaft is supported.

For the experiments in this paper, an estimator based on the cross-power spectrum techniques is selected due to its good performance if one assumes that SNR in the system input is

lower than the output SNR. That averaging method is also known in literature as H1, and can be expressed as:

$$\hat{G}_{H_1}(\omega_k) = \left(\frac{1}{N_b}\sum_{l=1}^{N_b} y_{(\omega_k)^{(l)}}\, u^*_{(\omega_k)^{(l)}}\right)\left(\frac{1}{N_b}\sum_{l=1}^{N_b} u_{(\omega_k)^{(l)}} u^*_{(\omega_k)^{(l)}}\right)^{-1} \quad (7)$$

where ω_k is the k-th frequency, $\mathcal{U}$ and $\mathcal{Y}$ are the input and output matrix, respectively. N_b is the number of blocks (repetitions) and l is the l-th block. Note that a proper input matrix (i.e. with all columns linearly independent) is a requirement to compute the right part of the Equation 7. Each column of the input and output matrix represents a different experiment, in which the excitation of one input at time is a typical method to build those matrices. In this way, the number of experiments be generally at least equal to the number of inputs. When the number of experiments is higher than that value, the Moore-Penrose inverse can be used to compute de estimator.

B. Excitation signal

The excitation signals are an important stage of identification procedures due to their influence in the experimental system signal to noise ratio measurements. The most common signal is the known stepped sine, which have a good SNR since the energy is stored in only the excited frequency [13]. When a real test rig parameter identification process is made, a range of frequencies is desired. One of the most important disadvantages of the previous signal is the time required to do the whole experiment [11]. Another way is use a multisine or multitoned signal, that is, an overlap of N_f sinusoidal signals at the same time, being expressed as:

$$S_e = \sum_{i=1}^{N_f} A_k cos(2\pi f_k t + \phi_k) \quad (8)$$

The previously mentioned works [8] [12] also evaluated the performance of some multisine signals, taking into account as an important variable the phases of the k-th harmonic component ϕ_k, highlighting the well behavior of the FRFs if the phases are selected using the equation proposed in Schroeder's paper[14], due to its relative low crest factor (approximately 1.8). For this reason, such a signal was chosen as the excitation input for this tests. Moreover, the frequencies were selected such that not excite below the fourth multiple of each frequency. This can be achieved by using the following expression [11]:

$$f_k = 4k + 1 \qquad k = k_0, k_1, \dots, k_{N_f} \quad (9)$$

As an example, in Figure 5 can be observed a multisine signal with Schroeder phases, flat amplitude and a total of 25 superposed frequencies. If one sets $k_0 = 2$, then the first frequency is $f_0 = 5Hz$, and the highest excited frequency will be $k_{N_f} = 101\ Hz$.

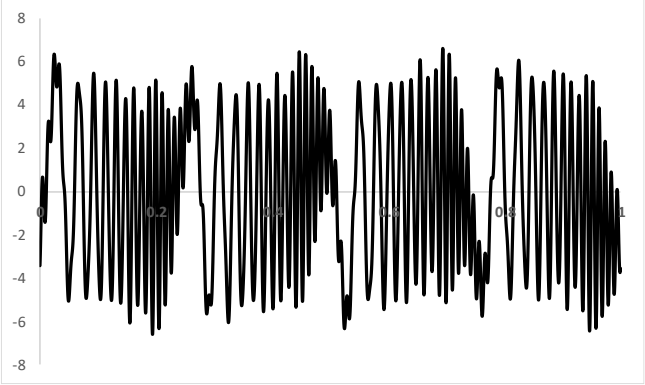

Figure 5. Multisine signal using Schroeder phases and flat amplitude ($A = 1\ V$), $k_0 = 2$ and $N_f = 25$

III. SMALL SCALE TEST RIG

A previous AMB small test rig was developed at the Acoustics and Vibrations Laboratory at the UFRJ by Siqueira [15] and then was improved by Coelho [16] (See Figure 6). In this test rig, the shaft is supported by an interaction between two eight heteropolar pole configuration (in differential arrangement) stators and a decentralized PID algorithm implemented in a CPU controller with FPGA (cRio-9030). That algorithm was developed in Labview environment,

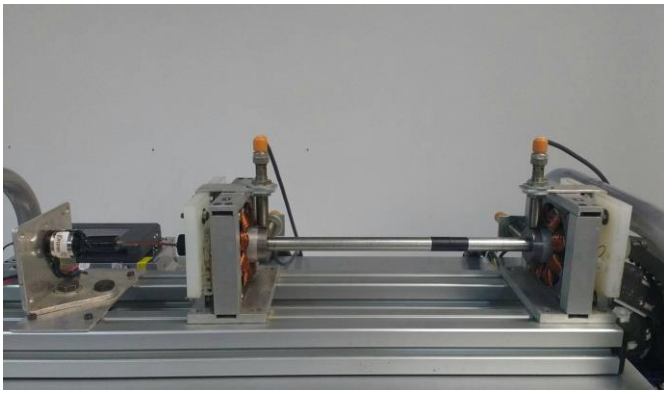

Figure 6. Small scale AMB prototype

allowing the manual tuning of controller gains, as well as a flexibility to making future controller scheme modifications.

Four inductive sensors (IFM IF6029) were installed in stator brackets in order to measure the shaft position. Those sensors were calibrated statically in a micrometer test rig. Similarly, a static calibration was performed for the current sensors (ACS712), using a calibrated current clamp meter.

Because the axial force is low if compared to the radial force, the axial load is supported by a flexible coupling that also serves as torque transmission between a brushless motor and the shaft. The motor speed is controlled by a NI myRio 1900 development board. The most relevant features of the AMB system are summarized in Table I.

TABLE I. SMALL-SCALE TEST RIG PARAMETERS

	Parameter	Value
m	Rotor mass	1 kg
L	Shaft length	400 mm
d_s	Shaft diameter	14.28 mm
d_j	Journal diameter	36.4mm
L_b	Bearing span between radial AMBs	315 mm
L_s	Distance between sensors	305 mm
C_g	Coil wire gauge	AWG 20
N_c	Turns per pole	130
I_b	Bias Current (average)	1.1 A
C_t	Core thickness	0.5 mm
B_{sat}	Magnetic flux density saturation	1.7 T
g_o	Nominal air gap	1 mm
A_g	Pole area	235 mm²
K_x	Negative position stiffness*	-2.11e4 N/m
K_i	Current stiffness*	21.14 N/A

* Predicted value

The original controller algorithm developed in the FPGA based system was modified in order to make possible the excitation signals [12], and an acquisition module (NI 9223) was added to the controller platform to receive those signals. A dedicated chassis (cDAQ 9178) with three modules of four analog inputs each one and an analog output module with four channels was used for excitation signal generation and identification purposes, as shown in Figure 7. An independent algorithm was devised for such a component, which allowed store the data in time domain and also in frequency domain. Finally, the averaging methods were applied using a previous developed Matlab script.

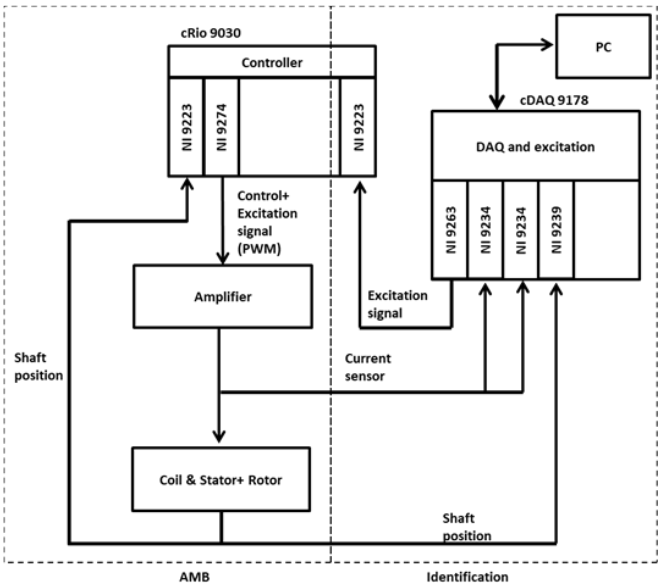

Figure 7. AMB system acquisition scheme

IV. EXPERIMENTAL RESULTS

The tests were performed considering the vertical and horizontal axis of the shaft displacement. The system was first excited in the horizontal axis and then in the vertical direction, producing a cylindrical movement. The net displacement of each axis was considered as the average of the both radial magnetic bearings, while the net perturbation currents are the sum of both bearing perturbation currents in each axis. With two inputs and two outputs, the frequency response function matrix can be represented as:

$$\begin{bmatrix} P_{x1} P_{x2} \\ P_{y1} P_{y2} \end{bmatrix} = \begin{bmatrix} G_{p_x i_x} & G_{p_x i_y} \\ G_{p_y i_x} & G_{p_y i_y} \end{bmatrix} \begin{bmatrix} I_{x1} I_{x2} \\ I_{y1} I_{y2} \end{bmatrix} \quad (10)$$

A total of 50 blocks were used to the FRF averaging process, where a convergence behavior of the frequency response curves was observed. A value of 5120 Hz was defined for acquisition rate, with 5120 samples, entailing a resolution of 1Hz. The applied signal excitation has a flat amplitude, and contains 50 tones with a broadband of 200 Hz. Figure 8 presents the calculated perturbation currents of the system for the horizontal and the vertical axes at 8400 RPM. The AMB is being excited in the horizontal direction. Therefore, the perturbation signal of the vertical axis is only composed by control current. The oscillations in that signal should

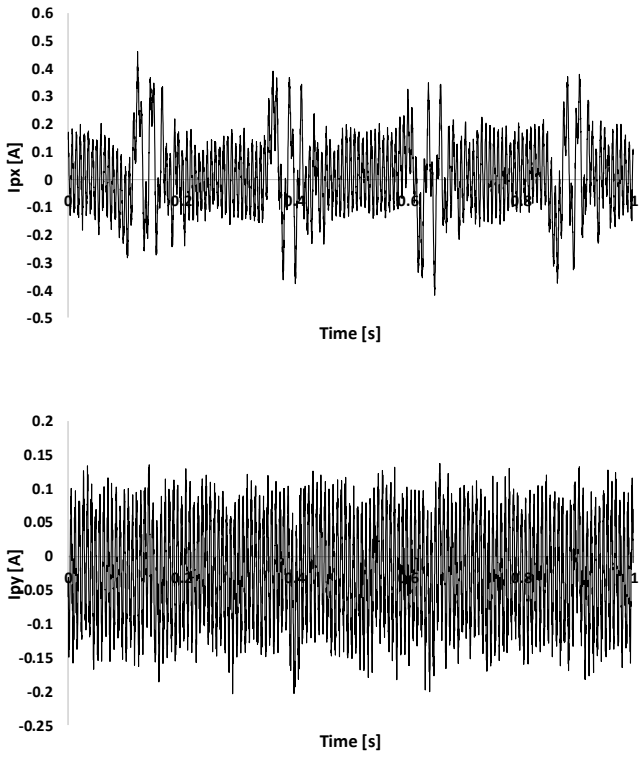

Figure 8. Current perturbation signals at 8400 RPM

correspond to the rotating speed of the shaft.

The measured shaft position at 8400 RPM is presented in Figure 9. One can perceive that displacement in the horizontal axis keeps in slightly lower order of magnitude of the vertical displacement. That behavior can be possible due to the flexible coupling, which is not strictly aligned with the shaft, also the gravity and likely a contribution of its residual unbalance.

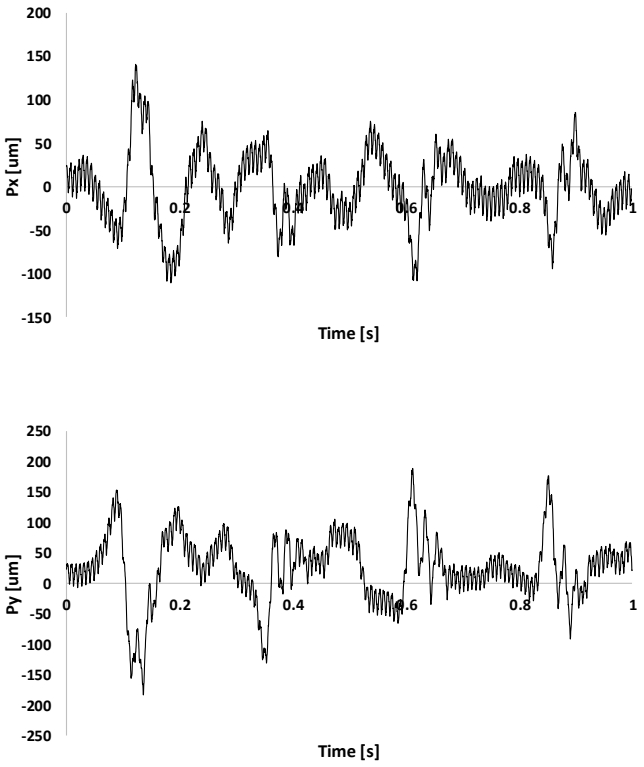

Figure 9. Position signals at 8400 RPM

With the purpose of taking a first sight in the frequency domain, the Discrete Fourier Transform is obtained for the input and output data. Figure 10 contains the spectrum of the outputs and inputs. The evenly spaced peaks correspond to the excited frequencies, and the highest value peak match the rotation speed.

In the input currents plot can be observed an attenuation as the frequency increases, since the excitation signal was set with a flat amplitude on all excited frequencies. This can occur due to the dynamic characteristics of amplifier, including their respective coil. Another observation that should be made is that the vertical current perturbation generates also frequencies even though its amplitude is lower. Definitely, the rotation speed is predominant in the spectrum, especially in the plant input.

Finally, the experiments were repeated for various rotating speeds, and their respective FRFs matrices were obtained, being summarized in Figure 11. It is possible to notice that the direct components ($G_{p_x i_x}$ and $G_{p_y i_y}$) have a lower discrepancy than cross-coupled components ($G_{p_y i_x}$ and $G_{p_x i_y}$). Moreover, the behavior of all the FRFs below the lowest rotation speed (3200 RPM) is very similar. The rotation generates also

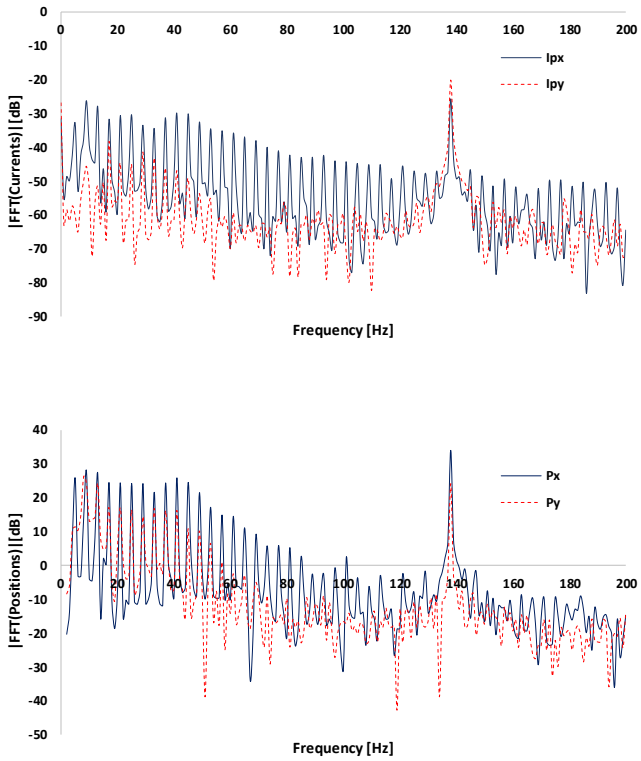

Figure 10. FFT of inputs and outputs of AMB plant at 8400 RPM

multiples of its own span frequency. Those multiples appear to be higher than the fundamental frequency. Outside the region of shaft rotation frequency and its harmonics, the FRF is very close to the response obtained in the nonrotating condition.

The phases of the FRFs are presented in Figure 12, where one can observe the same trend with the direct and cross-coupled components. In the case of the direct part, the values match with the theoretical model [10] (-180°) below approximately 90 Hz for nonrotating condition and 160 Hz for the other evaluated conditions. Above those frequencyies, the FRFs begin to oscillate. It likely can be due to the low SNR of the output at these frequencies, since the plant provokes an attenuation in the higher frequencies.

V. CONCLUSIONS

Unbalance and/or external shaft couplings can be significant in the identification procedures, since its effect may lead to mask the true results, when a model parametrization is the principal scope of the goal. As observed in the previous test, the unique case where the FRFs behaved in a similar way, was with the frequencies far away the rotation speed and its harmonics.

It is recommended to use the operational conditions as a “baseline” when a plant identification is carried out, in order to obtain an accurate result for any AMB application.

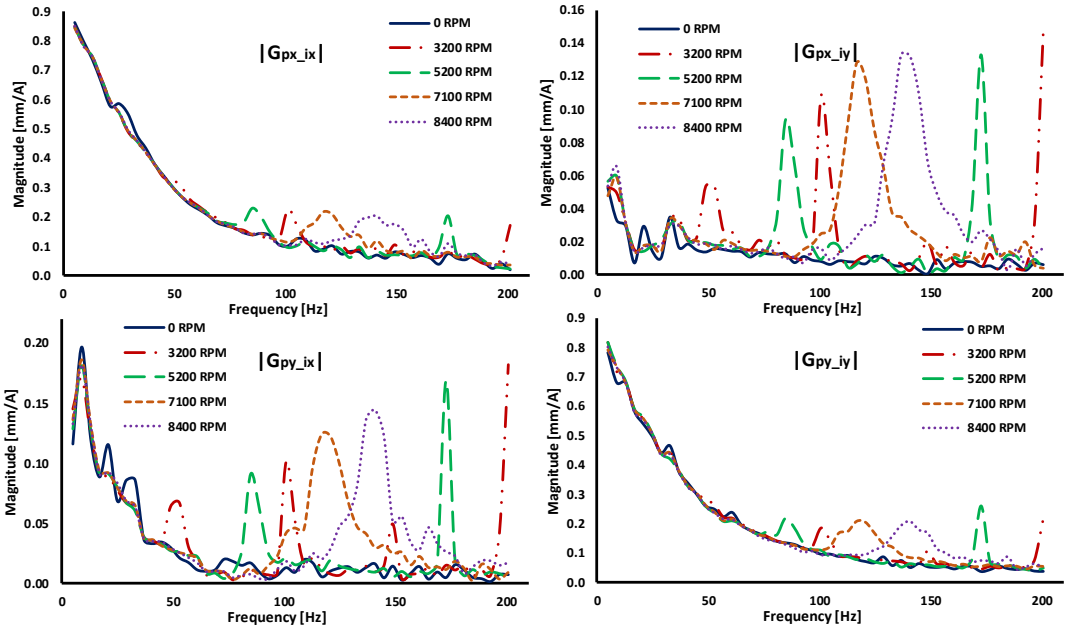

Figure 11. FRF magnitude of small-scale AMB test rig at several rotating speeds

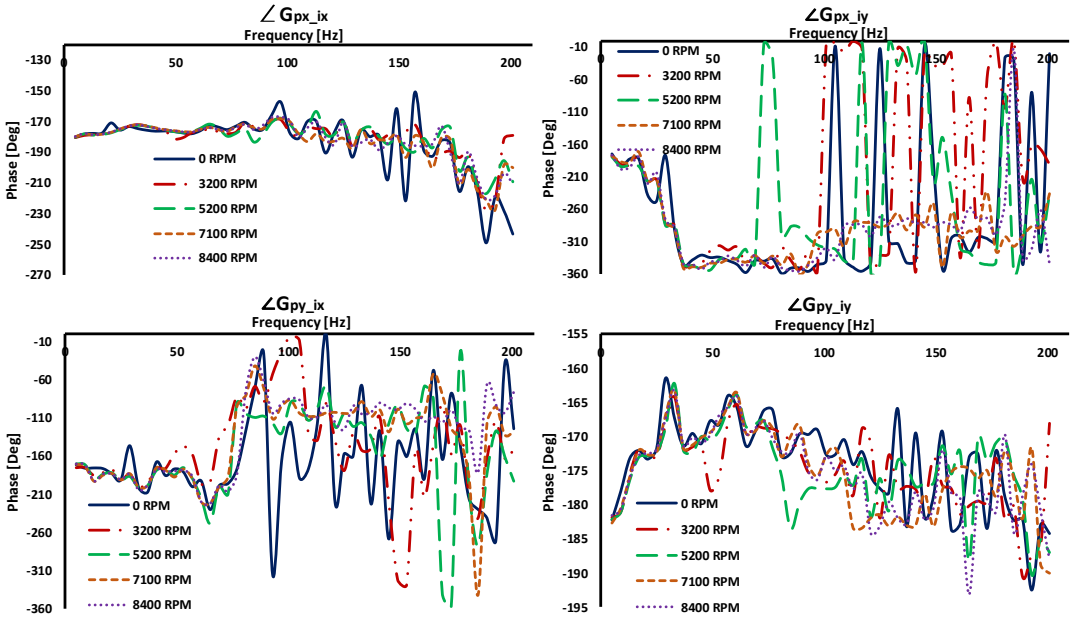

Figure 12. FRF phases of small-scale AMB test rig at several rotating speeds

For future works a parametric identification under several rotating speeds will be developed, and optimization algorithms will be applied, aiming reduce the number of blocks, and improving the excitation in the higher frequencies, where the attenuation is higher.

REFERENCES

[1] G. Schweitzer, "Active Magnetic Bearings – Chances and Limitations," Sydney, 2002.

[2] R. Nordmann, M. Matros e T. Neumer, "Parameter Identification in Rotating Machinery by Means of Active Magnetic Bearings," Chicago, 1994.

[3] N. G. Wagner e K. Steff, "Dynamic Labyrinth Coefficients from a High-Pressure Full-Scale Test Rig Using Magnetic Bearings," Texas, 1996.

[4] G. Vanini, S. Cioncolini, V. Calicchio e F. Tedone, "Development of a High Pressure Rotordynamic Test Rig for Centrifugal Compressors Internal Seals Characterization," *Proceedings of the Fortieth Turbomachinery Symposium*, Houston, Texas, 2011.

[5] C. Gälher e R. Herzog, “Identification of magnetic bearing systems,” *Mathematical and Computer Modelling of Dynamical Systems*, pp. 29-45, 1995.

[6] C. Gähler, M. Mohler e R. Herzog, “Multivariable Identification of Active Magnetic Bearing Systems,” *Van Campen D.H. (eds) IUTAM Symposium on Interaction between Dynamics and Control in Advanced Mechanical Systems*, vol. 52, pp. 127-134, 1997.

[7] H.-J. Ahn, D.-C. Han e E. Maslen, “Frequency Domains Identification of a MIMO AMB Rigid Rotos System Based on Measured Open-Loop Frequency Responses,” *Proceedings of ASME/IGTI Turbo Expo 2003*, Atlanta, Georgia, USA, 2003.

[8] K. Hynynen, “Broadband Excitation in the System Identification of Active Magnetic Bearing Rotor Systems,” Lappeenranta University of Technology., Lappeenranta., 2011.

[9] O. Turkay e A. G. Usloy, “Frequency Versus Time Domain Parameter Estimation: Application to a Slot Milling Operation,” *Mechanical Systems and Signal Processing*, vol. 2, nº 3, pp. 265-277, 1988.

[10] G. Schweitzer, E. M. Maslen e Ma, Magnetic Bearings: Theory, Design, and Application to Rotating Machinery, New York: Springer, 2009.

[11] R. Pintelon and J. Schoukens, System identification. A Frequency Domain Approach. 2 Ed, USA: Wiley, 2012.

[12] D. A. Diaz, F. A. Pinto, T. G. Ritto e D. j. Maldonado, “Stteped sine and Multisine Signal Excitation for Identification in a Small AMB Test Rig,” em *Proceedings of the 24th ABCM International Congress of Mechanical Engineering*, Curitiba, 2017.

[13] L. Ljung, System identification: Theory for User, New Jersey: Prentice Hall, 1987.

[14] M. Schroeder, “Synthesis of low peak factor signals and binary sequences with low autocorrelation,” *IEEE Transactions on Information Theory*, vol. 16, nº 1, pp. 85-89, Janeiro 1970.

[15] R. Siqueira, “Projeto e Implementação de um Mancal Magnético Ativo com Controle por Modos Deslizantes,” Federal University of Rio de Janeiro, Rio de Janeiro, 2013.

[16] J. Coelho, “Aspectos Mecânicos de Sistema de Mancais Magnéticos,” Federal University of Rio de Janeiro, Rio de Janeiro, 2016.

[17] R. Nordmann, “Identification Techniques in Rotordynamics,” *Diagnostics of Rotating Machines in Power Plants*, New York, Springer Verlag, 1994, pp. 1-24.